

Molecular-dynamics simulations on the crystallization of Fe metallic glasses under alternating magnetic field

Yanxue Wu(吴言雪), Qiang-Qiang Pan(潘强强), Rui Ning(宁睿), and Hailong Peng(彭海龙)
Citation: Chin. Phys. B, 2025, 34 (**7**): 076402. DOI: 10.1088/1674-1056/adc625
http://cpb.iphy.ac.cn; http://iopscience.iop.org/cpb

What follows is a list of articles you may be interested in

“Glass-quake” in elastically loaded bulk metallic glasses

Qi Huang(黄琦), Kaiguo Chen(陈开果), Chen Liu(刘辰), Guisen Liu(刘桂森), Yang Shao(邵洋), Chenlong Zhao(赵晨龙), Ran Chen(陈然), Hengtong Bu(卜亨通), Lingti Kong(孔令体), and Yao Shen(沈耀)
Chin. Phys. B, 2024, 33 (**11**): 116402. DOI: 10.1088/1674-1056/ad7725

Effect of overheating-induced minor addition on Zr-based metallic glasses

Fu Yang(杨福), Zhenxing Bo(薄振兴), Yao Huang(黄瑶), Yutian Wang(王雨田), Boyang Sun(孙博阳), Zhen Lu(鲁振), Baoan Sun(孙保安), Yanhui Liu(柳延辉), Weihua Wang(汪卫华), and Mingxiang Pan(潘明祥)
Chin. Phys. B, 2024, 33 (**3**): 036401. DOI: 10.1088/1674-1056/ad1823

A group of ductile metallic glasses prepared by modifying local structure of icosahedral quasicrystals

Qi Qiao(乔琪), Ji Wang(王吉), Zhengqing Cai(蔡正清), Shidong Feng(冯士东), Zhenqiang Song(宋贞强), Benke Huo(霍本科), Zijing Li(李子敬), and Li-Min Wang(王利民)
Chin. Phys. B, 2023, 32 (**11**): 116401. DOI: 10.1088/1674-1056/ace823

Effect of spatial heterogeneity on level of rejuvenation in $Ni_{80}P_{20}$ metallic glass

Tzu-Chia Chen, Mahyuddin KM Nasution, Abdullah Hasan Jabbar, Sarah Jawad Shoja, Waluyo Adi Siswanto, Sigiet Haryo Pranoto, Dmitry Bokov, Rustem Magizov, Yasser Fakri Mustafa, A. Surendar, Rustem Zalilov, Alexandr Sviderskiy, Alla Vorobeva, Dmitry Vorobyev, and Ahmed Alkhayyat
Chin. Phys. B, 2022, 31 (**9**): 096401. DOI: 10.1088/1674-1056/ac615e

Crystallization evolution and relaxation behavior of high entropy bulk metallic glasses using microalloying process

Danhong Li(李丹虹), Changyong Jiang(江昌勇), Hui Li(栗慧), and Mahander Pandey
Chin. Phys. B, 2021, 30 (**6**): 066401. DOI: 10.1088/1674-1056/abd92c

---

Molecular-dynamics simulations on the crystallization of Fe metallic glasses under alternating magnetic field

Yanxue Wu(吴言雪)[1], Qiang-Qiang Pan(潘强强)[1], Rui Ning(宁睿)[1], and Hailong Peng(彭海龙)[1,2,†]

[1] *School of Materials Science and Engineering, Central South University, Changsha* 410083, *China*
[2] *State Key Laboratory of Powder Metallurgy, Central South University, Changsha* 410083, *China*

(Received 12 March 2025; revised manuscript received 8 April 2025; accepted manuscript online 10 April 2025)

We performed the coupled molecular-dynamics and spin dynamics simulations to investigate the magnetic annealing effect on the crystallization behavior of Fe metallic glasses (MGs). By calculating the local five-fold symmetry, Voronoi polyhedron, and bond orientational order parameters, we find a significant structural evolution at high-frequency magnetic annealing: the icosahedral order diminishes, and the crystalline-like order is enhanced, comparing to the case without magnetic field. The fraction of the body-centered cubic structures remarkably increases with the frequency of magnetic annealing, and the atoms of these order show a tendency of aggregating in space to form the crystalline nuclei. These findings unveil how the local structure evolves under magnetic annealing, and the accelerated crystallization process of MGs through alternating magnetic fields.

Keywords: metallic glasses, magnetic annealing, crystallization behavior

PACS: 64.70.pe, 61.43.–j

DOI: 10.1088/1674-1056/adcb25 **CSTR:** 32038.14.CPB.adcb25

1. Introduction

Soft magnetic materials have wide applications in electric motors, transformers, radio electronic industry and so on. These typical materials include silicon steels (Fe–Si), permalloys (Fe–Ni), Hipperco 50 alloy (Fe–Co), metallic glasses and nanocrystalline composites.[1] Due to the nanoscale refinement of magnetic phase grain, nanocrystalline composites often exhibit superior performance characteristics, such as higher saturation magnetic field density, enhanced permeability, favorable high-frequency response, reduced energy losses, and improved thermal stability.[2] These exceptional properties endow them with strong competitive advantages, leading to widespread applications in magnetic cores for ground fault interrupters, common mode chokes and high frequency transformers.

One of the most common methods for producing a nanocrystalline alloy is by heating an amorphous precursor to induce crystallization and precipitate the nanocrystalline phase.[3] Amorphous alloys are usually produced as ribbons by rapid melt quenching onto a fast-moving substrate. Under subsequent treatment (heat treatment, deformation, laser treatment,[4] ultrasonic treatment,[5] etc.), a combined amorphous-crystalline structure can be formed.[6] For nanocrystals to be formed under crystallization, the process of crystallization must occur at a high rate of crystal nucleation and a low rate of crystal growth. From the perspective of thermodynamics, the transition from the amorphous phase to the nanocrystalline phase needs to overcome the energy barrier, which is affected by the external field.[7]

Considering the influence of pressure on nucleation thermodynamic barrier and phase transition, low-pressure stress annealing is a potential crystallization method for promoting crystallization, reducing the activation free energy required to form the crystal nucleus and decreasing the growth rate of nano-grains.[8] However, the unidirectional stress field causes anisotropic growth of nano-grains limiting the overall improvement of magnetic properties. Aiming to promote the nucleation rate of nanocrystals and decrease the growth rate of grains, the way of hot isostatic pressing (HIP)[9] and transverse or longitudinal magnetic annealing[10,11] proposed not only satisfy the requirements of the nano-grains but also optimize the soft magnetic properties simultaneously. Compared with HIP, magnetic field annealing not only promotes the formation of ordered structures but also reduces the unexpected field-induced magnetic anisotropy,[12] inducing uniaxial magnetic anisotropy,[13] especially under an alternating magnetic fields.[14] In particular, rotating magnetic annealing can even induce a critical-state amorphous structure, manifested as 1 nm-sized crystal-like orders sparsely dispersed in the amorphous systems,[15] enhancing the ferromagnetic exchange interactions[16] and improving the soft magnetic properties.[17]

The effects of glass composition and parameters of the crystallization process on the resulting structures[18,19] and magnetic properties were frequently studied in order to enable the preparation of magnetic materials with properties tai-

†Corresponding author. E-mail: hailong.peng@csu.edu.cn

© 2025 Chinese Physical Society and IOP Publishing Ltd. All rights, including for text and data mining, AI training, and similar technologies, are reserved.

lored for the respective application.[20] Thus, investigating the crystallization behavior of MG in different heat treatments is enlightening in obtaining the MG's phase compositions, microstructures and functional properties.[21]

Although the effect of the field annealing has been extensively studied on the properties of MGs, the consequence of the external magnetic field on the atomic-level structure is still unclear. Further in-depth studies are needed to understand the atomic structure change and their influence on crystallization behavior of amorphous alloys.

In this work, we explored the atomic structure evolution after magnetic field annealing with different parameters by the coupled molecular-dynamics and spin dynamics (MD-SDs) simulations on a pure-iron MGs system. The MD-SDs simulations constitute a classical magnetic spin modeling framework that incorporates classical spin vectors for individual magnetic moments alongside conventional positional and momentum coordinates. Considering a direct ferromagnetic exchange and interatomic potentials (IAPs) based on the first-principles calculations for magnetic iron to describe the magnetic properties. Based on this methodology, we constructed a model to simulate the effect of magnetic annealing on the crystallization behavior of MGs and clarified the structural evolution under the magnetic field.

2. Simulation details

We utilized the spin-lattice dynamics embedded in the large-scale atomic/molecular massively parallel simulator (LAMMPS)[22] through the symplectic and scalable algorithm,[23,24] which can be applied to describe the atomic spins in magnetic crystals from the ferromagnetic limit to the paramagnetic limit. In the system of magnetic spin interaction, the Hamiltonian can be written as

$$H(\boldsymbol{r}_i, \boldsymbol{p}_i, \boldsymbol{s}_i) = H_{\mathrm{mag}}(\boldsymbol{r}_i, \boldsymbol{s}_i) + \sum_{i=1}^{N} \frac{\boldsymbol{p}_i}{2m_i} + \sum_{i,j=1}^{N} V(r_{ij}), \quad (1)$$

where $\boldsymbol{r}_i$, $\boldsymbol{p}_i$, $\boldsymbol{s}_i$ and designate the atomic position, atomic momentum, the normalized magnetic moment, and the mass of atom i, respectively. $r_{i,j} = \boldsymbol{r}_i - \boldsymbol{p}_j$, is the interatomic distance between these two particles. is a mechanical potential. H_{mag} is the interatomic magnetic energy, and can be written as

$$H_{\mathrm{mag}} = -\sum_{i \neq j}^{N} J(r_{ij}) \left[\boldsymbol{s}_i \cdot \boldsymbol{s}_j - 1\right], \quad (2)$$

where $J(r_{ij})$ is the function defining the magnetic exchange interaction from neighboring shells, approximately fictionalized in the Bethe–Slater curve:[25]

$$f(r_{ij}) = 4a \left(\frac{r_{ij}}{d}\right)^2 \left[1 - b\left(\frac{r_{ij}}{d}\right)^2\right] \times \exp\left[-\frac{r_{ij}}{d}\right] \Theta(R_{\mathrm{c}} - r_{ij}), \quad (3)$$

where $\Theta(R_{\mathrm{c}} - r_{ij})$ is the Heaviside step function and R_{c} is the distance cutoff. Parameters a, b, and d are 25.498 meV, 0.281, and 1.999 Å respectively, based on the values for BCC iron.[26] Spin dynamics simulations are implemented within the microcanonical (NVE) ensemble, where the number of particles, volume, and total energy are conserved.[27,28] The temperature of kinetics and spin dynamics are controlled via Langevin dynamics separately. Spin temperature is scaled to ensure that the magnetization at different temperatures coincides with that of the experiments in the crystals [Fig. 1(a)].

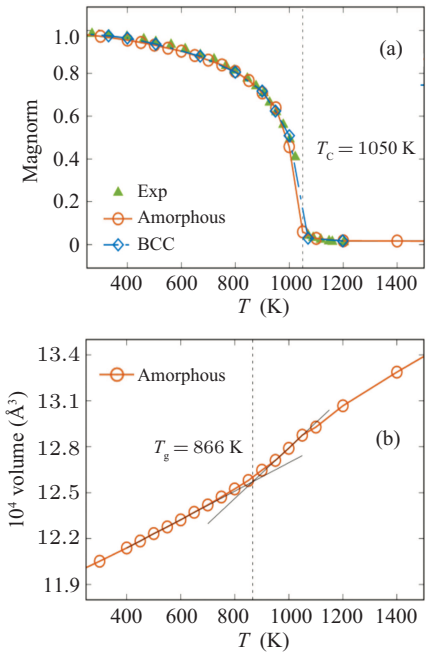


Fig. 1. (a) Variation of magnetization intensity in simulations with temperature for amorphous and BCC Fe. The fulfilled triangles are the experimental data for BCC irons.[29–33] The value at the inflection point is the Curie temperature. (b) Variation of simulated box volume with temperature for amorphous Fe during the cooling process.

In addition to the magnetic spin interactions, the mechanical interactions among atoms are described by the embedded atomic potential (EAM) method,[34] which not only fits the experimental parameters but also takes into account the results of first-principles calculations. The potential can accurately predict the lattice properties, surface energies and point defect energies for both BCC and the high temperature FCC phases of the metal.

The molecular dynamics system comprises 6000 atoms with periodic boundary conditions applied along all dimensions and an integration time step of 1 fs. Initial configurations were equilibrated at 2000 K followed by rapid quenching to 300 K at a cooling rate of 1.0×10^{13} K/s. The magnetic property of the amorphous Fe shows a close behavior with that of the crystalline Fe [Fig. 1(a)]. The glass transition temperature can be measured from the change in the volume of the simulated box with temperature [Fig. 1(b)].

The isothermal magnetic annealing process was simulated by providing a 1-T external magnetic field to amorphous

Fe, with a periodic reversal (T_p) of the field direction between the positive Z-axis and negative Z-axis. Four alternating field periods (i.e., $T_p = 2$ ps, 4 ps, 8 ps, and 20 ps) were investigated along with the zero-field annealing (ZFA) condition. All magnetic treatments were maintained for 1000 ps to ensure structural relaxation convergence. Specimens annealed at 500 K were selected for comparative analysis.

3. Results and discussion

The variation of the potential energy per atom under the applied magnetic field with different periods is shown in Fig. 2. The decay of this energy correlates with the glass-forming ability, which is the key indicator of the crystallization process. Generally, amorphous structures exhibit higher energy states compared to the metastable crystalline counterparts.[35] The energy elevation induced by the transition of the crystalline lattice from a thermodynamically stable configuration to a high-energy metastable state during the amorphization process, has been reported by molecular dynamics and first-principles calculations.[36] The crystallization process in magnetic systems can be monitored through potential energy variations under applied magnetic fields. A discontinuous shift in the potential energy profile typically indicates a first-order phase transition from amorphous to crystalline configuration, corresponding to structural reorganization at atomic scales. As is shown in Fig. 2, a noticeable reduction of the potential energies with T_p decreasing is observed. The smaller T_p has a stronger magnetic effect on the crystallization behavior. A stronger magnetic annealing can make the faster crystallization rate.

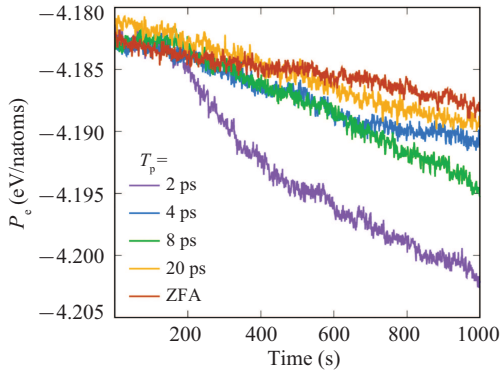


Fig. 2. The variation of potential energy with time for the different applied periodic magnetic fields.

To understand the change in the crystallization behavior, especially to explain the effect of magnetic annealing on the crystallization behavior of Fe MGs, we resort to the microscopic structure change induced by magnetic annealing. Figure 3 shows the results of the structural analysis for different periods of external magnetic fields. The structural indicator, local five-fold symmetry (LFFS), is an effective structural indicator to characterize the local structural feature of MGs.[37] The LFFS is defined as the fraction of the 5-edged faces in the Voronoi polyhedron,[38], i.e., $d_5 = n_5/\sum n_i$. For clusters with icosahedral (ICO) symmetry, which is the main local atomic structure in MGs,[39] d_5 is close to 1, whereas for clusters with crystalline symmetry (in which triple or quadruple symmetry dominates), d_5 is close to 0. The general structural feature of MG samples can be quantified by the average LFFS, $\bar{d}_5$, over all the atoms. The results were shown in Fig. 3(a), in which the average LFFS exhibits approximately an upward trend with T_p increasing. An increase of implies a more stable ICO order formed, whereas a decrease of indicates a more crystalline-like order formed.[40] This indicates that the number of clusters of more crystal-like symmetry increases upon magnetic annealing, relative to that in the ZFA samples. The population of crystalline-like clusters is the highest in the strongest magnetic annealing case ($T_p = 2$ ps).

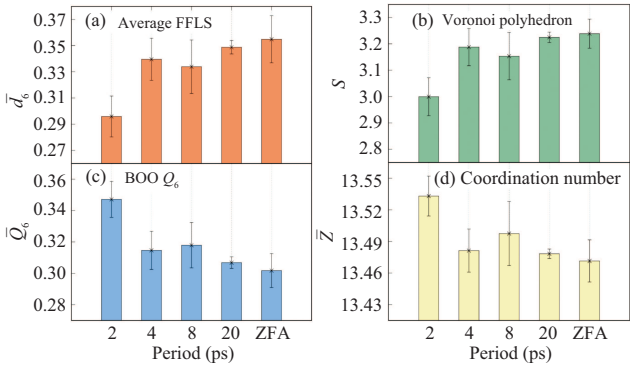


Fig. 3. The local structural evolution with T_p at 500 K, with (a) the average LFFS ($\bar{d}_5$), (b) the Voronoi entropy (S), (c) the average $\bar{Q}_6$ value of bond orientational order (BOO), and (d) the average coordination number ($\bar{Z}$) under different applied magnetic fields. The error bars come from the statistics of five independent samples.

To measure the local structural diversity or the disordering extent in the MGs, we calculated the structural entropy or Shannon entropy. The local configurational entropy can be calculated from the fraction of Voronoi polyhedron (P_i):[41]

$$S = -\sum_{i=1}^{N} P_i \log P_i. \tag{4}$$

When $S = 0$, the system is in the most ordered structure configuration. The higher the value of S, the more disordered the system is. Figure 3(b) shows the evolution of the calculated structural entropy in different periods of alternating magnetic fields. A monotonic evolution is observed: the structural entropy increases with the increasing period, and a maximum emerges at ZFA. Thus, the structure is more ordered in the samples of strong magnetic fields. The change of the LFFS and S is consistent with the change of potential energy with alternating magnetic fields as shown in Fig. 2. This indicates that LFFS and Voronoi entropy can well characterize the degree of crystallization behavior.

We also calculated the coarse-grained order parameter, Q_6, in bond orientational order (BOO) and the coordination

number (see Figs. 3(c) and 3(d)). Q_6 is an important parameter describing the local structural symmetry,[42] which can be used to separate atoms in the crystalline phase or the amorphous phase. It is calculated from the coordination projection of the neighboring atoms defined by the Voronoi tessellation onto the spherical harmonic functions,[43] as given in the following equation:

$$Q_6(i) = \sqrt{\frac{4\pi}{13}\sum_m \left| \frac{\sum_{j=1}^{N} f_i Y_6^m(\theta(r_{ij}))}{N_i + 1} \right|}, \tag{5}$$

where N_i is the number of the nearest neighbors of atom i, and $Y_6^m(\theta(r_{ij}))$ is the spherical harmonic with only considering the polar angles. f_i is the fraction of Voronoi polyhedral face area between i and j atoms over the overall face area. For clusters of crystalline orders, e.g., the hexagonal close-packed and the face-centered cubic structures, Q_6 is larger than 0.4; for clusters of liquid state, Q_6 is relatively smaller, about 0.16.[44] The atoms with Q_6 larger than 0.25 are considered to be potentially pre-orders in liquids (with crystalline-like symmetry).[45] The average value of Q_6, $\bar{Q}_6$, can be used to reflect the general structural over all the atoms. As shown in Fig. 3(c), the $\bar{Q}_6$ parameter shows a tendency of decrease with T_p increasing. The highest $\bar{Q}_6$ values at $T_p = 2$ ps verifies that the crystallization rate is the fastest and the local structure is the most crystalline like in the sample of the strongest magnetic annealing effect.

A consistent phenomenon can be observed from the results of the coordination number (see Fig. 3(d)), which is defined as the number of the nearest neighboring atoms in Voronoi polyhedra.[38] Crystalline structures exhibit statistically higher coordination numbers due to the close packing, whereas the amorphous structures display relatively smaller coordination numbers. The smaller coordination numbers in amorphous materials can be ascribed to the broken translational symmetry.[46] It can be found that with the decreasing period of the magnetic annealing, the coordination number increases, meaning the faster crystallization behavior.

These structural parameters provide the specific structure information of metallic glasses. To check the dependence of crystallization behavior on the magnetic fields, we alternatively analyze the crystalline order through the bond orientational order parameters,[42,47] from which the local clusters of a different order, e.g., the ICO order, hexagonal close packed (HCP) order, face-centered cubic (FCC) order, and body-centered cubic (BCC) order can be identified.[44,48] Figure 4 shows that the melts basically crystallized in all the samples, with the shorter period magnetic annealing significantly facilitating the formation of the crystalline structure, i.e., HCP, FCC, and BCC structures. Concomitantly, the ICO orders gradually disappear as the period decreases. This is consistent with the results of the local structure analysis shown in Fig. 3.

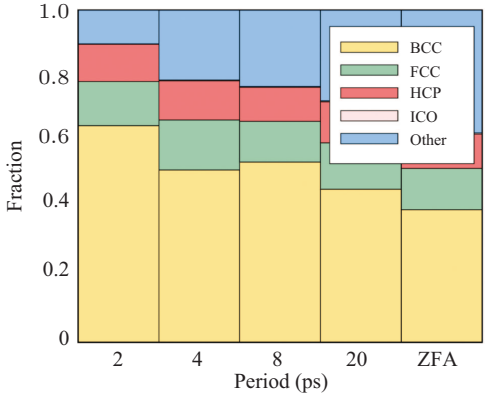


Fig. 4. Fraction of ICO, HCP, FCC, BCC, and disordered structures in the samples quenched to 500 K with different magnetic annealing T_p.

To compare the crystallization between different magnetic annealing, we visualized the atoms those are of the coarse-grained order parameter Q_6 more than 0.45 (shown in Fig. 5). As discussed before, the parameter of Q_6 can distinguish the crystalline-like and icosahedral-like orders. We found that the number of the visualized atoms approximately increases with the intensity of the magnetic field, i.e., 544, 592, 773, and 1335 atoms selected in case of ZFA, $T_p = 8$ ps, $T_p = 4$ ps, and $T_p = 2$ ps samples, respectively. These selected atoms show a tendency of aggregation in space and are of the BCC ordering, which indicates the crystal nucleation of the amorphous matrix. This, exactly, corresponds to the crystallized clusters found in Fig. 4. These results show that magnetic annealing plays an important role on the crystallization behavior in amorphous.

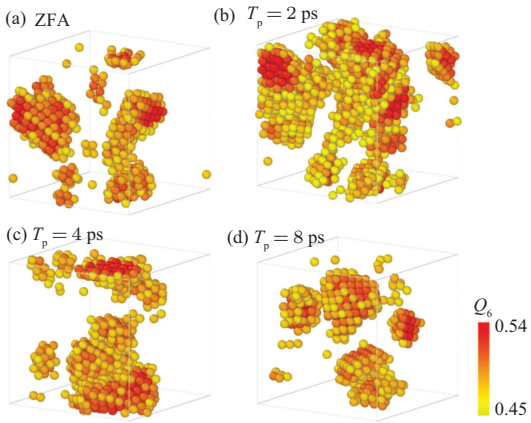


Fig. 5. Snapshot of atoms with the coarse-grained order parameter Q_6 larger than 0.45 at $T = 500$ K with (a) ZFA, (b) $T_p = 2$ ps, (c) $T_p = 4$ ps, and (d) $T_p = 8$ ps. The atoms are colored according to the value of Q_6.

4. Conclusion

In this work, we performed classical molecular-dynamics simulations to investigate the magnetic annealing effect on the crystallization behavior of Fe MGs and the associated structural evolution. The model can well capture the magnetic property of Fe metals in the isobaric ensemble. An alternating magnetic field is applied on the Fe MGs with different alternating periodicity or frequency. The results show that magnetic

annealing can enhance the kinetic process of crystallization. With increasing the magnetic frequency, the crystallization behavior becomes faster. The local structure is measured by the local five-fold symmetry, Voronoi entropy, the coarse-grained order parameter Q_6, and coordination numbers. These structural parameters show a monotonic behavior: the FFLS and structural entropy decrease with magnetic frequency, while Q_6 and coordination numbers increase, both indicating an enhancement of the translational order, or the crystalline-like order. Consistently, the results of the bond orientational order show that more crystalline structure is formed with shorter period magnetic annealing, for which the magnetic annealing effect is also stronger. The number of atoms that of crystalline order increases with magnetic frequency, and these atoms aggregates in space to form the crystalline nuclei. These results unveil the crystallization behavior tuned by magnetic annealing, and are helpful in understanding the mechanism of the structural evolution under magnetic fields.

Acknowledgments

Project supported by the Scientific Research Foundation of the Education Department of Hunan Province, China (Grant No. 24A0007), the National Natural Science Foundation of China (Grant No. 52371168), and the Foundation of Science and Technology on Surface Physics and Chemistry Laboratory (Grant No. JCKYS2024120202). We are also grateful to the computer resources provided by the High Performance Computing Cluster (HPC) of Central South University.

References

[1] Luo T, Huang M, Xu F, Liu H, Huang C, Yue G, Peng Z and Yang Y 2024 *J. Non-Cryst. Solids* **635** 122988
[2] Herzer G 2013 *Acta Mater.* **61** 718
[3] Azuma D, Ito N and Ohta M 2020 *J. Magn. Magn. Mater.* **501** 166373
[4] Zhang Y, Tong X, Yan Y, Cao S, Ke H B and Wang W H 2024 *Chin. Phys. B* **33** 108104
[5] Li W, Wang C, Li L, Zhang C, Ma J, Xi X, Tao K, Qiao J, Yuan C and Wang W 2025 *Int. J. Mech. Sci.* **287** 109960
[6] Abrosimova G, Volkov N, Pershina E, Chirkova V, Sholin I and Aronin A 2021 *J. Non-Cryst. Solids* **565** 120864
[7] Zhang X, Zhang F, Zhang J, Yu W, Zhang M, Zhao J, Liu R, Xu Y and Wang W 1998 *J. Appl. Phys.* **84** 1918
[8] Xu J, Liu X, Wang Y, Wang G, Wang J, Zhou L and Yang Y 2021 *J. Alloys Compd.* **882** 160746
[9] Xu J, Liu X, Wang Y, Shi Q, Wang J, Li K and Yang Y 2022 *J. Alloys Compd.* **902** 163887
[10] Wang C, Wu Z, Feng X, Li Z, Gu Y, Zhang Y, Tan X and Xu H 2020 *Intermetallics* **118** 106689
[11] Cheng Y and Ma E 2011 *Prog. Mater. Sci.* **56** 379
[12] Suzuki K and Herzer G 2012 *Scr. Mater.* **67** 548
[13] Hou L, Wang B, Liu L, Mao X, Zhang M, Yuan C, Li Z, Ju W, Feng H, Tang C, Xia A and Li W 2024 *J. Mater. Sci. Technol.* **200** 27
[14] Amirabadizadeh A, Mardani R and Ghanaatshoar M 2016 *J. Alloys Compd.* **661** 501
[15] Li H, Wang A, Liu T, Chen P, He A, Li Q, Luan J and Liu C T 2021 *Mater. Today* **42** 49
[16] Li X, Zhou J, Shen L, Sun B, Bai H and Wang W 2023 *Adv. Mater.* **35** 2205863
[17] Shao L, Bai R, Wu Y, Zhou J, Tong X, Peng H, Liang T, Li Z, Zeng Q and Zhang B 2024 *Mater. Futures* **3** 025301
[18] Wang B, Shang B S, Gao X Q, Sun Y T, Qiao J C, Wang W H, Pan M X and Guan P F 2022 *J. Non-Cryst. Solids* **576** 121247
[19] Liang S, Zhang L, Wang Y, Wang B, Pelletier J and Qiao J 2024 *Int. J. Fatigue* **187** 108446
[20] Zhang J, Zhou Z, Zhang Z, Park M, Yu Q, Li Z, Ma J, Wang A, Huang H and Song M 2022 *Mater. Futures* **1** 012001
[21] Harizanova R, Mihailova I, Georgieva M, Tzankov D, Cherkezova-Zheleva Z, Paneva D, Avramova I, Karashanova D, Avdeev G and Gugov I 2024 *J. Non-Cryst. Solids* **634** 122986
[22] Plimpton S 1995 *J. Comput. Phys.* **117** 1
[23] Ma P W, Dudarev S L and Woo C H 2016 *Comput. Phys. Commun.* **207** 350
[24] Tranchida J, Plimpton S J, Thibaudeau P and Thompson A P 2018 *J. Comput. Phys.* **372** 406
[25] Nieves P, Tranchida J, Arapan S and Legut D 2021 *Phys. Rev. B* **103** 094437
[26] Pajda M, Kudrnovský J, Turek I, Drchal V and Bruno P 2001 *Phys. Rev. B* **64** 174402
[27] Tranchida J, Plimpton S J, Thibaudeau P and Thompson A P 2018 *J. Comput. Phys.* **372** 406
[28] Garcí-Palacios J L and Lázaro F J 1998 *Phys. Rev. B* **58** 14937
[29] Wallace D C, Sidles P and Danielson G 1960 *J. Appl. Phys.* **31** 168
[30] Crangle J and Goodman G 1971 *Proc. R. Soc. London, A* **321** 477
[31] Seki I and Nagata K 2005 *ISIJ Int.* **45** 1789
[32] Basinski Z S, Hume-Rothery W and Sutton A 11955 *Proc. R. Soc. London, A* **229** 459
[33] Touloukian Y S 1970 *Thermophys. Prop. Mater.* **4** 83
[34] Chamati H, Papanicolaou N I, Mishin Y and Papaconstantopoulos D A 2006 *Surf. Sci.* **600** 1793
[35] Kalb J, Spaepen F and Wuttig M 2003 *J. Appl. Phys.* **93** 2389
[36] Da Silva J L, Walsh A, Wei S H and Lee H 2009 *J. Appl. Phys.* **106** 113509
[37] Peng H L, Li M Z and Wang W H 2011 *Phys. Rev. Lett.* **106** 135503
[38] Hirata A, Guan P, Fujita T, Hirotsu Y, Inoue A, Yavari A R, Sakurai T and Chen M 2011 *Nat. Mater.* **10** 28
[39] Qiao Q, Wang J, Cai Z, Feng S, Song Z, Huo B, Li Z and Wang L M 2023 *Chin. Phys. B* **32** 116401
[40] Ma L, Yang X D, Yang F, Zhou X J and Wu Z W 2024 *Chin. Phys. B* **33** 036402
[41] Peng H, Li M and Wang W 2013 *Appl. Phys. Lett.* **102** 131908
[42] Steinhardt P J, Nelson D R and Ronchetti M 1983 *Phys. Rev. B* **28** 784
[43] Rycroft C H 2009 *Chaos* **19** 041111
[44] Lechner W and Dellago C 2008 *J. Chem. Phys.* **129** 114707
[45] Hu Y C and Tanaka H 2022 *Nat. Commun.* **13** 4519
[46] Tong H, Tan P and Xu N 2015 *Sci. Rep.* **5** 15378
[47] Mickel W, Kapfer S C, Schröder-Turk G E and Mecke K 2013 *J. Chem. Phys.* **138** 044501
[48] Leocmach M and Tanaka H 2012 *Nat. Commun.* **3** 974